

Article

Optimizing Layer Thickness and Width for Fused Filament Fabrication of Polyvinyl Alcohol in Three-Dimensional Printing and Support Structures

Mahmoud Moradi ^{1,*}, Mojtaba Karamimoghadam ^{2,*}, Saleh Meiabadi ³, Shafqat Rasool ¹, Giuseppe Casalino ², Mahmoud Shamsborhan ⁴, Pranav Kattungal Sebastian ¹, Arun Poulouse ¹, Abijith Shaiju ¹ and Mohammad Rezayat ⁵

¹ Faculty of Arts, Science and Technology, University of Northampton, Northampton NN1 5PH, UK; shafqat.rasool@northampton.ac.uk (S.R.); pranavkattungal@gmail.com (P.K.S.); arunkoonathan@gmail.com (A.P.); abijithshaiju042@gmail.com (A.S.)

² Department of Mechanics, Mathematics and Management, Polytechnic University of Bari, Via Orabona 4, 70125 Bari, Italy; giuseppe.casalino@poliba.it

³ Department of Mechanical Engineering, École de Technologie Supérieure, 1100 Notre-Dame West, Montreal, QC H3C 1K3, Canada; mohammadsaleh.sheikhmohammadmeiabadi.1@ens.etsmtl.ca

⁴ Department of Mechanical Engineering, University of Zakho, Kurdistan Region 42001, Iraq; m.shamsborhan@gmail.com

⁵ Center for Structural Integrity, Micromechanics, and Reliability of Materials (CIEFMA)-Department of Materials Science and Engineering, Universitat Politècnica de Catalunya-BarcelonaTECH, 08019 Barcelona, Spain; mohammad.rezayat@upc.edu

* Correspondence: mahmoud.moradi@northampton.ac.uk (M.M.); m.karamimoghadam@phd.poliba.it (M.K.)



Citation: Moradi, M.; Karamimoghadam, M.; Meiabadi, S.; Rasool, S.; Casalino, G.; Shamsborhan, M.; Sebastian, P.K.; Poulouse, A.; Shaiju, A.; Rezayat, M. Optimizing Layer Thickness and Width for Fused Filament Fabrication of Polyvinyl Alcohol in Three-Dimensional Printing and Support Structures. *Machines* **2023**, *11*, 844. <https://doi.org/10.3390/machines11080844>

Academic Editors: Alessandro Greco, Donato Perfetto and Mario Caterino

Received: 29 July 2023

Revised: 14 August 2023

Accepted: 17 August 2023

Published: 19 August 2023



Copyright: © 2023 by the authors. Licensee MDPI, Basel, Switzerland. This article is an open access article distributed under the terms and conditions of the Creative Commons Attribution (CC BY) license (<https://creativecommons.org/licenses/by/4.0/>).

Abstract: Polyvinyl Alcohol (PVA) is frequently applied as a support material in 3D printing, especially in the crafting of intricate designs and projecting elements. It functions as a water-soluble filament, often paired with materials like ABS or PLA. PVA serves as a momentary scaffold, supporting the jutting segments of a 3D model throughout the printing process. Subsequent to printing, the primary component can be effortlessly isolated by dissolving the PVA support using water. PVA, being a pliable and eco-friendly polymer, is susceptible to moisture. Its aqueous solubility renders it a prime selection for bolstering 3D print structures. In this investigation, equivalent-sized samples were 3D printed utilizing an Ultimaker 3D printer to assess the potency of PVA-generated specimens. Tensile examinations were executed on each sample employing a testing apparatus. The durability of the specimens was notably impacted by the input parameters, specifically the stratum width and stratum thickness. Strength dwindled as stratum width increased, whereas it rose with augmented stratum thickness. A few specimens with heightened stratum width and compromised quality displayed subpar performance during the tensile assessment. The findings unveiled a peak tensile strength of 17.515 MPa and a maximum load of 1600 N. Attaining an optimal degree of material utilization led to a decrease in filament consumption by 8.87 g, all the while upholding a MTS (maximum tensile strength) of 10.078 MPa.

Keywords: Fused Filament Fabrication (FFF); Polyvinyl Alcohol (PVA); layer thickness; width thickness; 3D printing; tensile test

1. Introduction

Three-dimensional printing, also known as additive manufacturing (AM), involves the construction of three-dimensional objects from digital models by depositing, connecting, or solidifying material under computer control [1–3]. Unlike traditional manufacturing methods that involve material removal, 3D printing builds objects by layering materials [4–7]. The printing process involved dual extrusion and fused filament fabrication techniques. The quality and precision of the printed object were found to be influenced

by factors such as temperature management, material viscosity, layer adhesion, and the mechanical, thermal, and optical properties of the material [8–10]. Three-dimensional printing has revolutionized manufacturing by enabling rapid prototyping, shorter lead times, and the production of customized products. It has found applications in various industries, including healthcare, aerospace, defense, automotive, and education, facilitating innovation, efficiency, and experiential learning opportunities [11–14].

Sikidar et al. [15] investigated the effects of layer thickness on the mechanical characteristics of 3D-printed ABS polymer samples. They utilized a fused deposition modelling (FDM) 3D printing device to produce samples with varying layer thicknesses and compared them to a sample made through conventional injection molding. The results indicated that the samples produced via injection molding exhibited the highest values of tensile strength, impact strength, and hardness. Chaudhery et al. [16] comprehensively explored the 3D printing process, including methodology, materials, feed, technology, and applications. They introduced 3D/4D printing technologies and highlighted the use of PVA as a feedstock. The authors emphasized that traditional methods lacked the ability to produce complex structures, whereas 3D printing technologies, such as light-, droplet-, and extrusion-based systems, enabled their creation. The study also investigated the temperature response of PVA. Terranova et al. [17] investigated the synthesis of PVA-based nanocomposites using diamond nanograins as fillers and their application in 3D printing through additive manufacturing. They explored the use of PVA and detonation nanodiamond dispersions as innovative inks for layer-by-layer additive manufacturing of variously shaped objects. The researchers developed 3D printing technology and methods to shape hybrid materials while fabricating nanocomposites, utilizing PVA-DND inks as a test system. They emphasized the importance of aligning the chemical and physical properties of the materials with the 3D printer to enhance the quality of the final printed products. The study demonstrated that well-defined and shaped structures of PVA-DND nanocomposites can be successfully printed, offering potential applications across various fields. Dwiwati et al. [18] conducted research on the axial and lateral tensile characteristics of Acrylonitrile Butadiene Styrene (ABS) material for 3D printing. Specimens were printed with varying layer thicknesses of 0.1, 0.2, and 0.3 mm, following ASTM D 632-02 standards [19]. Tensile tests were performed using the Zwick Roell Series Z 021 machine, and SEM testing was used to analyze the fracture surface. The study concluded that the axial direction of 3D-printed specimens exhibited higher maximum force and tensile strength compared to the lateral direction, with thicker layers more likely to exhibit greater maximum force and tensile strength. Yu et al. [20] investigated the mechanical behavior of 3D preforms and their composites produced via additive manufacturing, focusing on the influence of printing direction. The compressive behavior of 3D braid preforms, and composites was analyzed for three different printing orientations (0° , 45° , and Z-direction). Pores induced by the fabrication process were observed in sections printed at 0° and 45° orientations. Solid cube specimens were then created and injected with a silicone matrix. Preforms printed in the 45° direction exhibited improved inter-yarn adhesion, leading to enhanced initial modulus. However, Z-direction specimens displayed greater structural ductility due to inter-yarn slippage. Paul et al. [21] explored the application of novel biomaterials and advanced 3D printing techniques in bioprinting. The study highlights recent advancements in 3D printing technology and new materials, emphasizing their superiority over traditional methods, particularly in the field of biomedicine. Key considerations discussed include printing speed, feasibility of cell growth, and the ability to achieve complex shapes in bioprinting applications. Several studies have been conducted to investigate the mechanical properties of 3D-printed samples made from polyvinyl alcohol (PVA) and establish a correlation between printer parameters and mechanical characteristics [22–27]. These research efforts aim to understand how variations in printer settings, such as layer thickness, infill density, and printing speed, affect the resulting mechanical properties of PVA-based 3D-printed objects [28–32]. By identifying these relationships, researchers can optimize printer parameters to achieve desired mechanical properties in PVA 3D-printed samples [33–36]. AM,

particularly Material Extrusion (MEX), refers to a swift and convenient manufacturing technique that employs raw materials in filament structure. It holds the potential to effectively utilize recycled plastics and fibers sourced from industrial waste and household recycling, making it a viable approach for sustainability [37,38].

This study explores various methods employed in 3D printing technologies, specifically utilizing a dual extrusion print head and fused filament fabrication. The objective is to investigate the influence of input parameters, including layer thickness and wall thickness, on the strength of specimens. To conduct the experiment, shape samples were produced using PVA as the material on an Ultimaker 3D printer, while adhering to the specified input parameters. Subsequently, measurements were taken from the output samples and subjected to a tensile test. Results were obtained through graphical analysis, providing insights into material strength and force analysis. Furthermore, optimization and design of experiments were applied, utilizing the response surface method to optimize the weight and maximum tensile strength of the 3D-printed samples. The goal is to enhance the weight efficiency and mechanical characteristics of PVA samples subsequent to the 3D printing procedure.

2. Experimental Work

The experiment aimed to use an Ultimaker 5 3D printer to construct samples and investigate the impact of layer thickness and width thickness on their mechanical properties. The process involved creating a 3D design using SolidWorks software (version 11) and converting it into a series of cross-sectional layers. Fused filament fabrication (FFF) technology was employed, where a molten material was layered to build the items. Thermoplastic polymers like ABS and Nylon were used, and a dual extrusion print head with an auto nozzle lifting system was utilized. PVA material was prepared by being feed into the printer's filament spool and then into the print head, and the parameters were defined based on the response surface method levels (Table 1). In this study, the selected infill pattern was the honeycomb design. The specimens were fabricated following the dimensions specified for the ISO 527-2 tensile test samples [39].

Table 1. Independent process parameters with design levels.

Variable	Notation	Unit	−2	−1	0	1	2
Layer thickness	LT	[mm]	0.1	0.15	0.2	0.25	0.3
Width thickness	WT	[mm]	0.4	0.6	0.8	1	1.2

Table 2 provides the chemical properties of PVA. The printing process involved extruding PVA layer by layer to form the shape of the object. In some cases, support structures were used and later removed. Once printing was completed, the product was removed from the print bed and any remaining support structures were taken out. The samples were then subjected to tensile testing to analyze their mechanical properties.

Table 2. Chemical properties of PVA.

Formula	(C ₂ H ₄ O) _x
Melting Point	200 °C
Density	1.19 g/cm ³
Boiling Point	228 °C
Solubility in	Water
EPA	DTXSID431930
Log P	0.26

After the completion of 3D printing, additional post-processing steps can be performed to improve the surface quality of the object, including sanding or polishing. The removal of PVA support material is achieved by submerging the printed object in water, causing

the PVA to dissolve and leaving behind the primary 3D-printed component. Once dried, the part may require further post-processing, such as sanding or finishing, to achieve the desired outcome. The result is a 3D-printed object constructed by PVA materials. This procedure was repeated to produce a total of eleven samples, and the final products can be observed in Figure 1. Geometrical parameters, including weight, length, and thickness, were measured for each sample (Table 3). Subsequently, all the 3D-printed samples underwent tensile strength testing using an Instron 5567 Universal Testing Machine (UTM). The nozzle temperature was set within the range of 180 to 280 degrees Celsius with a nozzle diameter of 0.6 mm.

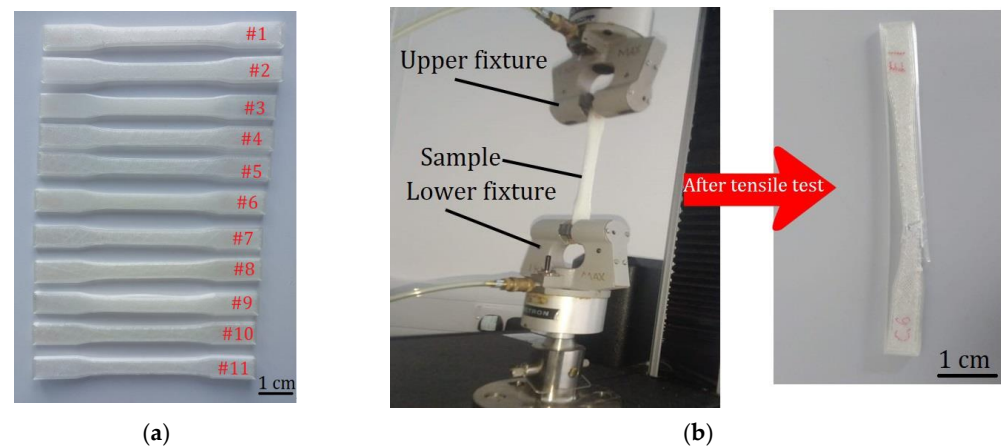


Figure 1. (a) Final products (3D-printed object made with PVA material). (b) The samples during and after tensile testing.

Table 3. Experimental layout and multi-performance results.

Experiment No.	Input Variables		Responses	
	LT [mm]	WT [mm]	MTS (MPA)	Weight (g)
1	0.2	1.2	8.892	8.34
2	0.25	0.6	13.878	9.26
3	0.2	0.4	17.515	9.40
4	0.2	0.8	12.708	9.58
5	0.2	0.8	14.175	9.68
6	0.1	0.8	13.431	9.46
7	0.3	0.8	14.507	9.47
8	0.15	0.6	17.925	9.68
9	0.15	1	10.458	8.83
10	0.2	0.8	14.587	9.40
11	0.25	1	4.417	7.95

3. Result and Discussion

3.1. Maximum Tensile Strength (MTS)

The ANOVA Table 4 presents the designed model for the MTS of the samples after 3D printing. In this model, the effects of input parameters on the MTS are analyzed. Based on the p -values and the significant model experiments, the effects of the parameters are deemed significant. Referring to the ANOVA Table 4 and the coefficients Equation (1), it

can be concluded that the effects of the WT parameter on the MTS are greater compared to the effects of the LT parameter in the printed samples.

$$(\text{MTS})^{2.26} = +1090.15231 - 560.87673 \times \text{LT} - 768.57399 \times \text{WT} \quad (1)$$

Table 4. Analysis of variance (ANOVA) for MTS.

Source	Sum of Squares	df	Mean Square	F Value	p-Value Prob > F
Model	2.930×10^5	2	1.465×10^5	13.39	0.0028
A-LT	9437.48	1	9437.48	0.86	0.3802
B-WT	2.835×10^5	1	2.835×10^5	25.91	0.0009
Residual	87530.92	8	10941.36		
Lack of Fit	80375.07	6	13395.84	3.74	0.2258
Pure Error	7155.85	2	3577.93		
Cor Total	3.805×10^5	10			

In Figure 2, the output graphs generated by the “Design Expert” software for the printed sample’s MTS are displayed. Figure 2a represents the normal plot of residuals for the MTS, showing that the residuals align closely with the trend line, indicating the conformity of the DOE for this output. Figure 2b, which is the perturbation plot for the MTS, examines the simultaneous effects of two parameters, WT and LT, on the MTS of the samples. Figure 2c presents the surface plot for the MTS of the samples. Based on this plot and the 2D contour plot of the MTS (Figure 2d), it can be observed that the MTS increases with a decrease in the WT of the printer. This is because reducing the WT results in thinner printed layers, leading to better filament consolidation in the samples. Increased consolidation of the printed layers requires more force to separate the samples, ultimately resulting in an increase in the MTS. Furthermore, considering the red regions in Figure 2d, the MTS of the samples is maximized when the WT parameter is set to a lower value for the printer. This is because decreasing the WT increases the print density and filament consumption, which leads to an increase in the MTS of the samples.

The tensile test results were obtained using a computer-controlled tensile testing machine. The results were analyzed and presented in the form of graphs. In Figure 3a, the load applied to sample 1 is plotted against the corresponding extension. It is evident that the sample exhibits elastic behavior up to an extension of 1.75 mm with a force of 510 N. Beyond this point, the material deviates from its elastic state. The maximum load observed is 760 N, achieved at a stretch of 3 mm. Subsequently, as the sample is stretched further, a decrease in force is observed until fracture occurs at a 7 mm extension. Similarly, in Figure 3b, the load applied to sample 2 is plotted against the extension. The graph shows that the sample retains its elastic properties up to an extension of approximately 1.00 mm, with a force of around 500 N. Upon exceeding this limit, the material loses its elastic behavior. The maximum load recorded is 1050 N at an extension of 2.5 mm. As the sample is stretched beyond this point, a decrease in force is observed until the sample fractures at an extension of over 7.25 mm. Comparing the results of sample 1 and sample 2, it is noteworthy that sample 2, which was printed with a layer thickness of 0.25 mm and width thickness of 0.6 mm, exhibited a 36 percent increase in maximum load and a 56 percent increase in the MTS of Elasticity compared to sample 1. Furthermore, the width thickness of sample 2 was reduced to half of that in sample 1.

3.2. Weight

In ANOVA, Table 5, the designed model for the weight of the samples after 3D printing is presented. In this model, the effects of the input parameters on the weight of the samples, as well as the second-order effects of WT, are analyzed. Based on the p-values, the effects of the parameters and the experimental model are found to be significant. Considering ANOVA, Table 5, and the coefficients Equation (2), it can be concluded that the effects of

the WT parameter on the weight of the printed samples are greater compared to the effects of the LT parameter.

$$(\text{Weight})^3 = +655.92146 - 489.41132 \times \text{LT} + 1087.08498 \times \text{WT} - 942.73992 \times \text{WT}^2 \quad (2)$$

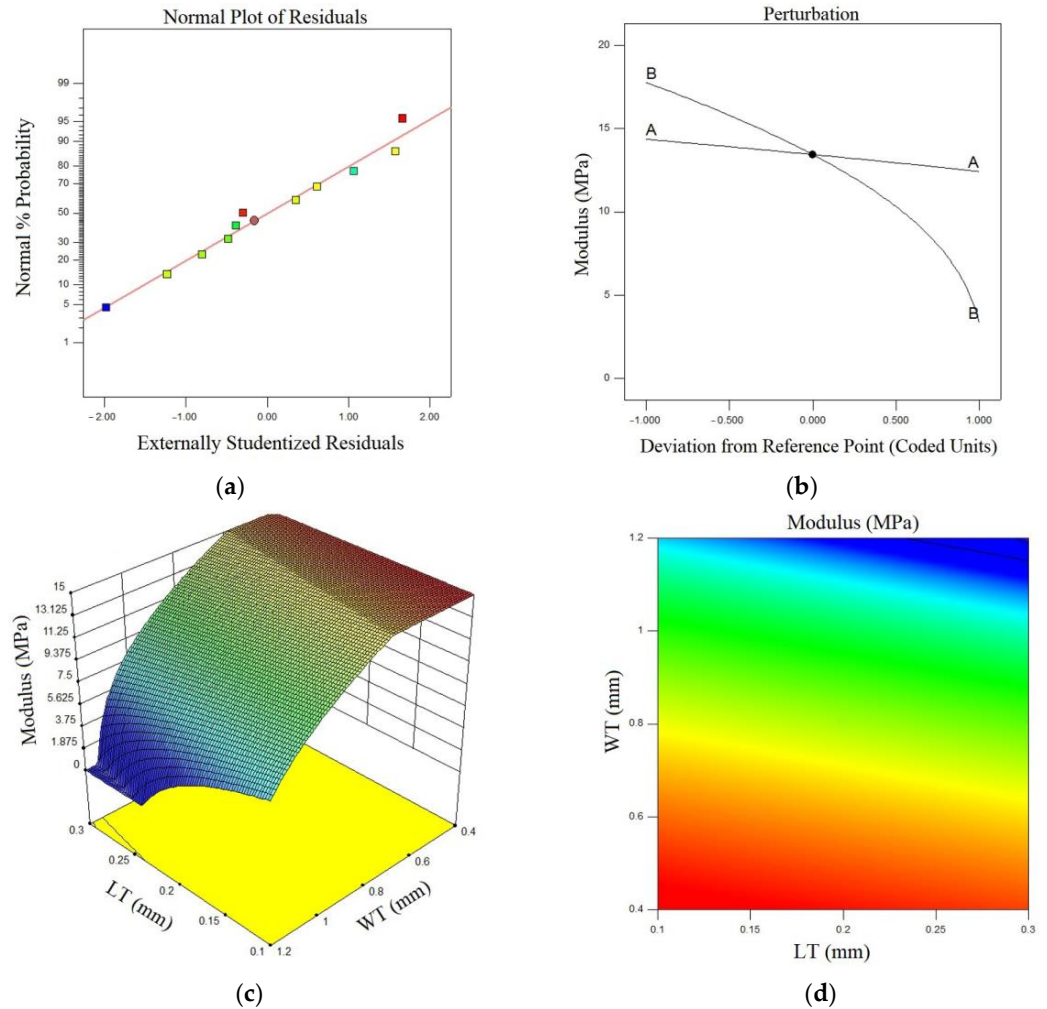


Figure 2. (a) Normal plot of residuals of MTS (b) Perturbation plot of MTS (c) 3D surface plot of MTS in terms of LT and WT (d) contour plot of MTS.

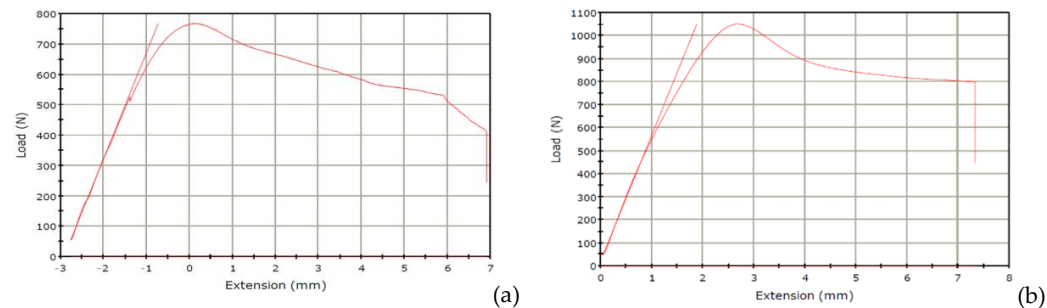


Figure 3. (a) Load (N) vs. Extension (mm) of Sample 1 (b) Load (N) vs. Extension (mm) of Sample 2.

In Figure 4, the output graphs of the Design Expert software (version 11) for the weight of the printed samples are shown. In Figure 4a, the normal plot of residuals for weight is displayed, indicating the residuals align closely to the diagonal line, indicating the adequacy of the DOE for this output. In Figure 4b, the surface plot for weight is presented. Based on this plot and the 2D contour plot of weight (Figure 4c), it can be observed that

increasing the weight of the samples is directly related to an increase in LT. This is because an increase in LT leads to thicker printed layers, resulting in higher filament consumption and ultimately increasing the weight of the samples. Additionally, considering the red regions in Figure 4c, the weight of the samples is minimized when the WT parameter is low and the LT parameter is set on high for the printer, as reducing WT increases print density and filament consumption, leading to an increase in sample weight.

Table 5. Analysis of variance (ANOVA) for Weight.

Source	Sum of Squares	Df	Mean Square	F Value	<i>p</i> -Value Prob > F
Model	1.250×10^5	3	41,653.09	5.12	0.0348
A-LT	7185.70	1	7185.70	0.88	0.3787
B-WT	85,196.52	1	85,196.52	10.47	0.0143
B ²	32,577.04	1	32,577.04	4.00	0.0855
Residual	56,966.61	7	8138.09		
Lack of Fit	53,971.72	5	10,794.34	7.21	0.1263
Pure Error	2994.90	2	1497.45		
Cor Total	1.819×10^5	10			

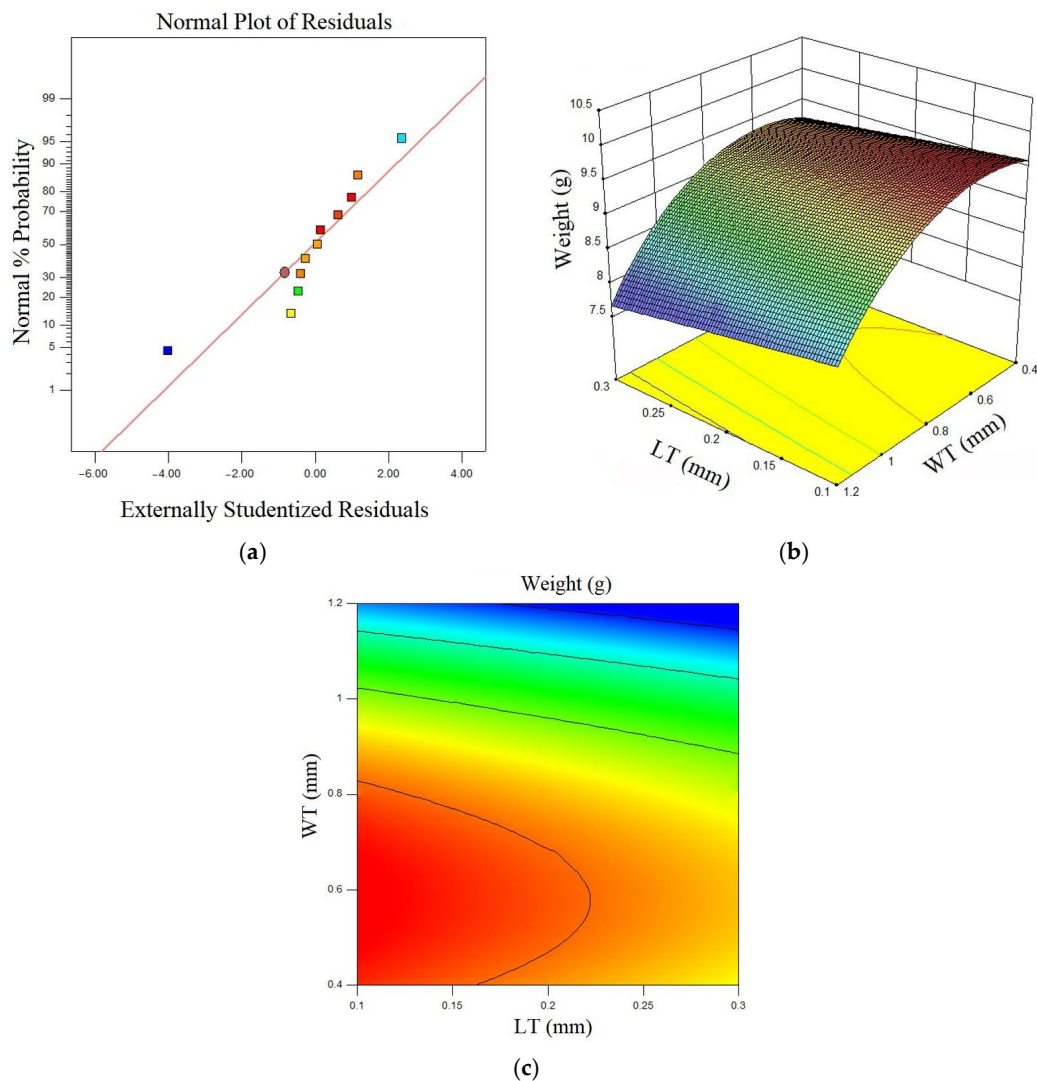


Figure 4. (a) Normal plot of residuals of Weight; (b) 3D surface plot of Weight in terms of LT and WT (c) contour plot of Weight.

4. Optimization

In this section, the optimization of 3D-printed PVA samples using the FFF method is addressed. In this optimization, two input parameters of the printer, namely WT and LT, were optimized based on the optimization Table 6, where the parameter ranges for both samples were evaluated, considering the upper and lower limits. Since the responses for this study are MTS and Weight, a goal was set for each in the optimization analysis, aiming to increase the MTS and decrease the Weight of the printed PVA samples. Furthermore, according to Table 7, three optimized samples were shown for this experiment, and the predicted values by the Design Expert software and the actual data from the tests were reported for these three optimized samples. As evident, the error values for the samples are below 15%, which is highly suitable for predicting the optimization of the samples based on previous studies, and conducted research. Additionally, considering the overlay plot in Figure 5, it demonstrates the optimized regions for the input parameters of the printer, where selecting a parameter within the yellow regions will result in optimal responses.

Table 6. Constraints and criteria of input parameters and responses.

Name	Goal	Lower Limit	Upper Limit	Lower Weight	Upper Weight	Importance
A: LT	is in range	0.1	0.3	1	1	3
B: WT	is in range	0.4	1.2	1	1	3
MTS	maximize	4.41779	17.925	1	1	3
Weight	minimize	7.95	9.68	1	1	3

Table 7. Predicted optimum results and experimental validation.

No.	LT	WT	Desirability	MTS (MPa)	Weight (g)
#1	0.3	0.85	1	Predicted	13.540
				Actual	11.985
				Error %	12.97
#2	0.25	0.85	0.953	Predicted	11.603
				Actual	12.091
				Error %	4.03
#3	0.25	0.95	0.947	Predicted	10.815
				Actual	10.078
				Error %	7.31

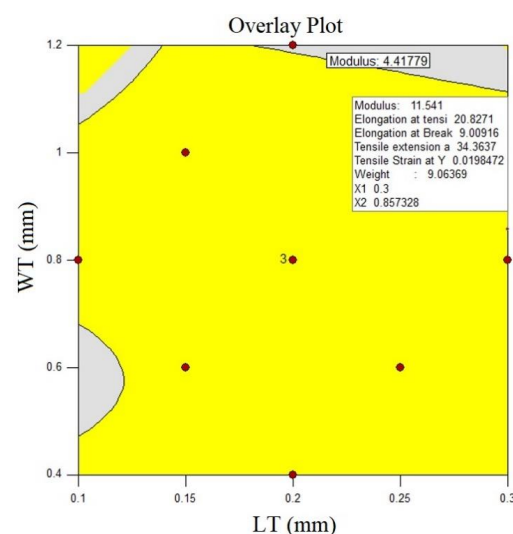


Figure 5. Overlay plots in terms of LT and WT.

5. Conclusions

The constraints and future potential of PVA 3D printing encompass its susceptibility to moisture, causing degradation, print issues, and extruder clogs, necessitating proper storage. Primarily used as support material in dual-extrusion 3D printing, PVAs limited application excludes standalone objects due to properties and cost. Slower print speeds increase project duration, deterring time-sensitive tasks. Higher cost hampers larger projects and cost-effectiveness goals. Its biocompatibility is promising for temporary medical implants. PVA finds utility in education and rapid prototyping due to easy support removal. Anticipated technological advancements could alleviate limitations and expand prospects as researchers strive to optimize PVA-based 3D printing for diverse applications. Below are notable accomplishments from this research:

- Mechanical properties of printed samples were significantly influenced by the width thickness parameter.
- Low layer thickness and high width thickness combo reduces tensile strength due to poor layer adhesion in width direction.
- Using 0.25 mm layer thickness and 1 mm width thickness requires less material but increases voids and lowers tensile strength.
- Sample 8: 0.15 mm layer thickness, 0.6 mm width thickness, MTS of 17.925 MPa.
- Sample 3: 0.2 mm layer thickness, 0.4 mm width thickness, MTS of 17.515 MPa, maximum load 1600 N. Sample 3 maintains good MTS with a reduced filament consumption of 8.87 g (10.078 MPa).

Author Contributions: Conceptualization, M.M. and M.K.; methodology, M.M., M.K., S.M., G.C., S.R., M.S. and M.R.; software, S.M.; validation, P.K.S., A.P., S.M. and M.S.; formal analysis, S.M.; investigation, M.M., A.S. and G.C.; Experimental work and data curation, P.K.S., S.R., A.P., A.S. and M.M.; writing—original draft preparation, M.K. and S.M.; writing—review and editing, M.M., M.K., G.C., M.S. and M.R.; visualization, M.M., M.K., S.M., G.C., M.S. and M.R.; supervision, M.M., G.C. and M.K. All authors have read and agreed to the published version of the manuscript.

Funding: This research received no external funding.

Data Availability Statement: Data detail is already provided in the contents of this paper.

Conflicts of Interest: The authors declare no conflict of interest.

Abbreviations

FFF	Fused filament fabrication
DOE	Design of Experiment
RSM	Response Surface Methodology
PVA	Polyvinyl Alcohol
ANOVA	Analysis of Variance
ABS	Acrylonitrile Butadiene Styrene
LT	Layer thickness
WT	Width thickness
UTM	Universal Testing Machine
MTS	Maximum Tensile Strength

References

1. Nazir, A.; Gokcekaya, O.; Billah, K.M.M.; Ertugrul, O.; Jiang, J.; Sun, J.; Hussain, S. Multi-material additive manufacturing: A systematic review of design, properties, applications, challenges, and 3D Printing of materials and cellular metamaterials. *Mater. Des.* **2023**, *226*, 111661. [[CrossRef](#)]
2. Moradi, M.; Karami Moghadam, M.; Shamsborhan, M.; Bodaghi, M. The synergic effects of FDM 3D printing parameters on mechanical behaviors of bronze poly lactic acid composites. *J. Compos. Sci.* **2020**, *4*, 17. [[CrossRef](#)]
3. Ouassil, S.E.; El Magri, A.; Vanaei, H.R.; Vaudreuil, S. Investigating the effect of printing conditions and annealing on the porosity and tensile behavior of 3D-printed polyetherimide material in Z-direction. *J. Appl. Polym. Sci.* **2023**, *140*, e53353. [[CrossRef](#)]

4. Al-Dulaijan, Y.A.; Alsulaimi, L.; Alotaibi, R.; Alboainain, A.; Akhtar, S.; Khan, S.Q.; Al-Ghamdi, M.; Gad, M.M. Effect of Printing Orientation and Postcuring Time on the Flexural Strength of 3D-Printed Resins. *J. Prosthodont.* **2023**, *32*, 45–52. [[CrossRef](#)] [[PubMed](#)]
5. Kara, Y.; Kovács, N.K.; Nagy-György, P.; Boros, R.; Molnár, K. A novel method and printhead for 3D printing combined nano-/microfiber solid structures. *Addit. Manuf.* **2023**, *61*, 103315. [[CrossRef](#)]
6. Meiabadi, M.S.; Moradi, M.; Karamimoghadam, M.; Ardabili, S.; Bodaghi, M.; Shokri, M.; Mosavi, A.H. Modeling the producibility of 3D printing in polylactic acid using artificial neural networks and fused filament fabrication. *Polymers* **2021**, *13*, 3219. [[CrossRef](#)]
7. Tomal, W.; Kiliclar, H.C.; Fiedor, P.; Ortyl, J.; Yagci, Y. Visible light induced high resolution and swift 3D printing system by halogen atom transfer. *Macromol. Rapid Commun.* **2023**, *44*, 2200661. [[CrossRef](#)]
8. An, Z.; Liu, Z.; Mo, H.; Hu, L.; Li, H.; Xu, D.; Chitrakar, B. Preparation of Pickering emulsion gel stabilized by tea residue protein/xanthan gum particles and its application in 3D printing. *J. Food Eng.* **2023**, *343*, 111378. [[CrossRef](#)]
9. Dey, D.; Panda, B. An experimental study of thermal performance of 3D printed concrete slabs. *Mater. Lett.* **2023**, *330*, 133273. [[CrossRef](#)]
10. Moradi, M.; Karami Moghadam, M.; Shamsborhan, M.; Bodaghi, M.; Falavandi, H. Post-processing of FDM 3D-printed polylactic acid parts by laser beam cutting. *Polymers* **2020**, *12*, 550. [[CrossRef](#)]
11. Zhang, X.N.; Zheng, Q.; Wu, Z.L. Recent advances in 3D printing of tough hydrogels: A review. *Compos. Part B Eng.* **2022**, *238*, 109895. [[CrossRef](#)]
12. Zhong, H.; Zhang, M. 3D printing geopolymers: A review. *Cem. Concr. Compos.* **2022**, *128*, 104455. [[CrossRef](#)]
13. Zhu, Y.; Tang, T.; Zhao, S.; Joralmon, D.; Poit, Z.; Ahire, B.; Keshav, S.; Rajee, A.R.; Blair, J.; Zhang, Z.; et al. Recent advancements and applications in 3D printing of functional optics. *Addit. Manuf.* **2022**, *52*, 102682. [[CrossRef](#)]
14. Zhang, F.; Li, Z.; Xu, M.; Wang, S.; Li, N.; Yang, J. A review of 3D printed porous ceramics. *J. Eur. Ceram. Soc.* **2022**, *42*, 3351–3373. [[CrossRef](#)]
15. Shubham, P.; Sikidar, A.; Chand, T. The influence of layer thickness on mechanical properties of the 3D printed ABS polymer by fused deposition modeling. *Key Eng. Mater.* **2016**, *706*, 63–67. [[CrossRef](#)]
16. Mallakpour, S.; Tabesh, F.; Hussain, C.M. A new trend of using poly (vinyl alcohol) in 3D and 4D printing technologies: Process and applications. *Adv. Colloid Interface Sci.* **2022**, *301*, 102605. [[CrossRef](#)]
17. Angjellari, M.; Tamburri, E.; Montaina, L.; Natali, M.; Passeri, D.; Rossi, M.; Terranova, M.L. Beyond the concepts of nanocomposite and 3D printing: PVA and nanodiamonds for layer-by-layer additive manufacturing. *Mater. Des.* **2017**, *119*, 12–21. [[CrossRef](#)]
18. Dwiayati, S.T.; Kholil, A.; Riyadi, R.; Putra, S.E. Influence of layer thickness and 3D printing direction on tensile properties of ABS material. *J. Phys. Conf. Ser.* **2019**, *1402*, 066014. [[CrossRef](#)]
19. Rajpurohit, S.R.; Dave, H.K. Tensile Properties of 3D Printed PLA under Unidirectional and Bidirectional Raster Angle: A Comparative Study. *Int. J. Mater. Metall. Eng.* **2018**, *22*, 6–11.
20. Quan, Z.; Suhr, J.; Yu, J.; Qin, X.; Cotton, C.; Mirotnik, M.; Chou, T.W. Printing direction dependence of mechanical behavior of additively manufactured 3D preforms and composites. *Compos. Struct.* **2018**, *184*, 917–923. [[CrossRef](#)]
21. Pradeep, P.V.; Paul, L. Review on novel biomaterials and innovative 3D printing techniques in biomedical applications. *Mater. Today Proc.* **2022**, *58*, 96–103. [[CrossRef](#)]
22. Stammen, J.A.; Williams, S.; Ku, D.N.; Guldborg, R.E. Mechanical properties of a novel PVA hydrogel in shear and unconfined compression. *Biomaterials* **2001**, *22*, 799–806. [[CrossRef](#)] [[PubMed](#)]
23. Kamran, M.; Saxena, A. A comprehensive study on 3D printing technology. *MIT Int. J. Mech. Eng.* **2016**, *6*, 63–69.
24. Hema, M.; Selvasekerapandian, S.; Hirankumar, G.; Sakunthala, A.; Arunkumar, D.; Nithya, H. Structural and thermal studies of PVA: NH4I. *J. Phys. Chem. Solids* **2009**, *70*, 1098–1103. [[CrossRef](#)]
25. Markiz, N.; Horváth, E.; Ficzer, P. Influence of printing direction on 3D printed ABS specimens. *Prod. Eng. Arch.* **2020**, *26*, 127–130. [[CrossRef](#)]
26. Noushini, A.; Samali, B.; Vessalas, K. Effect of polyvinyl alcohol (PVA) fibre on dynamic and material properties of fibre reinforced concrete. *Constr. Build. Mater.* **2013**, *49*, 374–383. [[CrossRef](#)]
27. Prabhakar, M.M.; Saravanan, A.K.; Lenin, A.H.; Mayandi, K.; Ramalingam, P.S. A short review on 3D printing methods, process parameters and materials. *Mater. Today Proc.* **2021**, *45*, 6108–6114. [[CrossRef](#)]
28. Liu, B.; Liu, X.; Li, G.; Geng, S.; Li, Z.; Weng, Y.; Qian, K. Study on anisotropy of 3D printing PVA fiber reinforced concrete using destructive and non-destructive testing methods. *Case Stud. Constr. Mater.* **2022**, *17*, e01519. [[CrossRef](#)]
29. Teodorescu, M.; Bercea, M.; Morariu, S. Biomaterials of PVA and PVP in medical and pharmaceutical applications: Perspectives and challenges. *Biotechnol. Adv.* **2019**, *37*, 109–131. [[CrossRef](#)]
30. Struzziero, G.; Barbezat, M.; Skordos, A.A. Assessment of the benefits of 3D printing of advanced thermosetting composites using process simulation and numerical optimisation. *Addit. Manuf.* **2023**, *63*, 103417. [[CrossRef](#)]
31. Wang, Q.; Zhang, G.; Zheng, X.; Ni, Y.; Liu, F.; Liu, Y.; Xu, L.R. Efficient characterization on the interlayer shear strengths of 3D printing polymers. *J. Mater. Res. Technol.* **2023**, *22*, 2768–2780. [[CrossRef](#)]
32. Aki, D.; Ulag, S.; Unal, S.; Sengor, M.; Ekren, N.; Lin, C.C.; Yilmazer, H.; Ustundag, C.B.; Kalaskar, D.M.; Gunduz, O. 3D printing of PVA/hexagonal boron nitride/bacterial cellulose composite scaffolds for bone tissue engineering. *Mater. Des.* **2020**, *196*, 109094. [[CrossRef](#)]

33. Hua, W.; Shi, W.; Mitchell, K.; Raymond, L.; Coulter, R.; Zhao, D.; Jin, Y. 3D printing of biodegradable polymer vascular stents: A review. *Chin. J. Mech. Eng. Addit. Manuf. Front.* **2022**, *1*, 100020. [[CrossRef](#)]
34. Baniasadi, H.; Madani, Z.; Ajdary, R.; Rojas, O.J.; Seppälä, J. Ascorbic acid-loaded polyvinyl alcohol/cellulose nanofibril hydrogels as precursors for 3D printed materials. *Mater. Sci. Eng. C* **2021**, *130*, 112424. [[CrossRef](#)]
35. Rovetta, R.; Pallavicini, A.; Ginestra, P.S. Bioprinting process optimization: Case study on PVA (Polyvinyl Alcohol) and Graphene Oxide biocompatible hydrogels. *Procedia CIRP* **2022**, *110*, 145–149. [[CrossRef](#)]
36. Moradi, M.; Karamimoghadam, M.; Meiabadi, S.; Casalino, G.; Ghaleeh, M.; Baby, B.; Ganapathi, H.; Jose, J.; Abdulla, M.S.; Tallon, P.; et al. Mathematical modelling of fused deposition modeling (FDM) 3D printing of poly vinyl alcohol parts through statistical design of experiments approach. *Mathematics* **2023**, *11*, 3022. [[CrossRef](#)]
37. Sam-Daliri, O.; Ghabezi, P.; Flanagan, T.; Finnegan, W.; Mitchell, S.; Harrison, N.M. Recovery of Particle Reinforced Composite 3D Printing Filament from Recycled Industrial Polypropylene and Glass Fibre Waste. *Proc. World Congr. Mech. Chem. Mater. Eng.* **2022**, *177*, 3–4.
38. Ghabezi, P.; Flanagan, T.; Harrison, N. Short basalt fibre reinforced recycled polypropylene filaments for 3D printing. *Mater. Lett.* **2022**, *326*, 132942. [[CrossRef](#)]
39. Yao, T.; Deng, Z.; Zhang, K.; Li, S. A method to predict the ultimate tensile strength of 3D printing polylactic acid (PLA) materials with different printing orientations. *Compos. Part B Eng.* **2019**, *163*, 393–402. [[CrossRef](#)]

Disclaimer/Publisher’s Note: The statements, opinions and data contained in all publications are solely those of the individual author(s) and contributor(s) and not of MDPI and/or the editor(s). MDPI and/or the editor(s) disclaim responsibility for any injury to people or property resulting from any ideas, methods, instructions or products referred to in the content.